Molecular Basis of Proton Block of L-Type Ca²⁺ Channels

Xiao-Hua Chen, Ilya Bezprozvanny, and Richard W. Tsien

From the Department of Molecular and Cellular Physiology, Stanford University, Stanford California 94305

ABSTRACT Hydrogen ions are important regulators of ion flux through voltage-gated Ca²⁺ channels but their site of action has been controversial. To identify molecular determinants of proton block of L-type Ca²⁺ channels, we combined site-directed mutagenesis and unitary current recordings from wild-type (WT) and mutant L-type Ca²⁺ channels expressed in *Xenopus* oocytes. WT channels in 150 mM K⁺ displayed two conductance states, deprotonated (140 pS) and protonated (45 pS), as found previously in native L-type Ca²⁺ channels. Proton block was altered in a unique fashion by mutation of each of the four P-region glutamates (E*I*–E*IV*) that form the locus of high affinity Ca²⁺ interaction. Glu(E) → Gln(Q) substitution in either repeats *I* or *III* abolished the high-conductance state, as if the titration site had become permanently protonated. While the E*I*Q mutant displayed only an ∼40 pS conductance, the E*III*Q mutant showed the ∼40 pS conductance plus additional pH-sensitive transitions to an even lower conductance level. The E*IV*Q mutant exhibited the same deprotonated and protonated conductance states as WT, but with an accelerated rate of deprotonation. The E*II*Q mutant was unusual in exhibiting three conductance states (∼145, 102, 50 pS, respectively). Occupancy of the low conductance state increased with external acidification, albeit much higher proton concentration was required than for WT. In contrast, the equilibrium between medium and high conductance levels was apparently pH-insensitive. We concluded that the protonation site in L-type Ca²⁺ channels lies within the pore and is formed by a combination of conserved P-region glutamates in repeats *I*, *II*, and *III*, acting in concert. E*IV* lies to the cytoplasmic side of the site but exerts an additional stabilizing influence on protonation, most likely via electrostatic interaction. These findings are likely to hold for all voltage-gated Ca²⁺ channels and provide a simple molecular explanation for the modulatory effect of H⁺ ions on open channel flux and the competition between H⁺ ions and permeant divalent cations. The characteristics of H⁺ interactions advanced our picture of the functional interplay between P-region glutamates, with important implications for the mechanism of Ca²⁺ selectivity and permeation.

KEY WORDS: ion channels • protonation • P-region • permeation • *Xenopus* oocytes

INTRODUCTION

Extracellular pH falls sharply during episodes of intense neuronal activity (Chesler and Kaila, 1992) or with ischemia in brain or heart (Katz, 1992; Siesjo et al., 1993). The change in pH₀ has an significant effect on many kinds of ion channels (Hille, 1992; Traynelis, 1996). However, the mechanism of pH-dependent control of channel function is not completely understood at the molecular level. Voltage-gated calcium channels are particularly interesting targets of hydrogen ion regulation because of their biological importance as a delivery system for a key intracellular messenger. Increased [H⁺] strongly inhibits ion permeation through open Ca²⁺ channels as well as reducing channel opening (Prod'hom et al., 1987; Krafte and Kass, 1988; Klöckner and Isenberg, 1994). The inhibitory effect of extracellular acidification on voltage-gated Ca²⁺ channels helps limit Ca²⁺ overload and subsequent damage during a metabolic insult (e.g., Ou-Yang et al., 1994).

Ilya Bezprozvanny's present address is Department of Physiology, The University of Texas Southwestern Medical Center at Dallas, 5323 Harry Hines Blvd., Dallas, Tx 75235-9040.

Address correspondence to Dr. Richard W. Tsien, Department of Molecular and Cellular Physiology, Beckman Center, B105A, Stanford, CA 94305-5426. Fax: 415-725-8021; E-mail: rwtsien@leland.stanford.edu

The interaction between protons and Ca²⁺ channels also shows intriguing biophysical properties. Recordings of unitary currents through L-type Ca²⁺ channels by the late Peter Hess and colleagues provided the first direct measurements of the protonation/deprotonation rates of a single molecule (Prod'hom et al., 1987). When probed with various monovalent cations as charge carriers, these channels were protonated at a single site with an anomalously high affinity for H⁺ (pK$_a$ > 7.0), resulting in an unusual subconductance state (Prod'hom et al., 1987; Pietrobon et al., 1989; Prod'hom et al., 1989). Protons also reduced the unitary fluxes of Ca²⁺ and other divalent cations, although much greater acidification was required for block (Krafte and Kass, 1988; Kuo and Hess, 1993; Klockner and Isenberg, 1994).

Despite extensive study, disagreement remains about the locus of H⁺ block of Ca²⁺ channels and the mechanism of inhibition of ion flux. In the prevailing hypothesis, Hess and colleagues proposed that protons titrate an external histidine residue, outside of the permeation pathway, and reduce channel conductance by an allosteric mechanism (Pietrobon et al., 1989). Mutagenesis studies have provided direct support for such an allosteric mechanism in the case of proton block of

inward rectifier K^+ channels (Coulter et al., 1995). However, an alternative possibility of H^+ block of Ca^{2+} channels is that the protonation site resides within the pore itself and that ion movements are reduced by a straightforward blocking mechanism (Kuo and Hess, 1993). This hypothesis gains plausibility by analogy to cyclic nucleotide gated (CNG)[1] channels (Root and MacKinnon, 1994). H^+ block of CNG channels involves glutamates in the pore-forming region (Root and MacKinnon, 1994), homologous to residues that form the high-affinity Ca^{2+} binding site in Ca^{2+} channels (Kim et al., 1993; Tang et al., 1993; Yang et al., 1993; Ellinor et al., 1995).

We set out to resolve these questions, using a combination of site-directed mutagenesis and single channel recordings from *Xenopus* oocytes expressing wild-type (WT) and mutated L-type Ca^{2+} channels. Our experiments provided direct evidence that protons block the Ca^{2+} channel by interacting with a site along the permeation pathway, rather than an external regulatory site outside of the pore. The observations allowed us to identify a specific subset of P-region glutamates that make up the protonation site and led to a simple explanation of how carboxylate side chains of these glutamates work in concert to form a single titration site with extremely high H^+ affinity. The proton interactions gave fresh perspective on the asymmetrical disposition of the P-region glutamates, and their possible conformational flexibility, relevant to fundamental mechanisms of Ca^{2+} channel selectivity and ion permeation.

METHODS

Expression of the Wild-type and Mutant L-type Ca^{2+} Channels in Xenopus Oocytes

L-type channels were expressed in *Xenopus* oocytes in the subunit combination $\alpha_{1C}\beta_{2b}\alpha_2$ as described previously (Yang et al., 1993; Ellinor et al., 1995). Briefly, the corresponding cRNAs were generated by in vitro transcription using rabbit clones for α_{1C} (Mikami et al., 1989), β_{2b} (Hullin et al., 1992), and α_2 (Mikami et al., 1989), and coinjected in *Xenopus* oocytes in approximately equal molar ratio. Expression of the L-type Ca^{2+} channels was confirmed by the appearance of FPL 64176-sensitive Ba^{2+} current in whole oocyte recordings using the two-electrode voltage clamp. The experiments were usually performed 4–5 d after the cRNA injection. The single glutamate to glutamine mutations in the P-region of L-type Ca^{2+} were generated as previously described by Yang et al. (1993). Using the original constructs (Yang et al., 1993), single channel recordings for several mutants were difficult due to the relatively low density of L-type channels expressed on the sur-

face of *Xenopus* oocytes. We increased the level of channel expression more than threefold by truncating part of the 5'-untranslated region. Thus, most of the single channel recordings were performed with the modified constructs.

Single Channel Recordings

The vitelline membrane was manually removed from the oocytes expressing wild-type or mutant L-type channels immediately before patch-clamp experiments using a published procedure (Methfessel et al., 1986; Sather et al., 1993). Cell-attached patch-clamp recording was performed on oocytes bathed in $\sim$100 mM K^+ solution (in mM, 100 KCl, 10 HEPES, 10 EGTA, 11 $MgCl_2$, pH 7.2 with KOH). In most experiments, the patch-clamp pipette was filled with KCl solution prepared in ^2H_2O (in mM, 150 KCl, 5 EDTA). In some cases, 150 mM NaCl solution prepared in either ^2H_2O or H_2O was used instead of KCl. The pipette solution also contained 5 mM pH buffer, either HEPES (for pH 7.5 and 8.5) or CHES (for pH 9.75), and was titrated with HCl to the desired pH. The p^2H value was obtained as the pH meter reading + 0.4 (Perrin and Dempsey, 1974). In all the experiments, the L-type Ca^{2+} channel agonist FPL 64176 (5 μM) was included in both pipette and bath solutions to prolong channel openings.

The unitary currents were recorded using an Axopatch 200 amplifier (Axon Instruments, Foster City, CA), filtered at 5 kHz and sampled at 25 kHz. Membrane potential was held at -100 mV, and stepped to various test voltages ranging from -40 to -120 mV. In some experiments, a brief prepulse to a strongly positive voltage was applied before the test pulse to facilitate channel opening. Single channel recordings were corrected offline for linear leak and capacity current by subtracting averaged blank records. Computer programs for data acquisition and analysis were written in AxoBasic. All experiments were conducted at room temperature (21–23°C).

Data Analysis

Long channel openings were manually selected and pooled together from multiple sweeps for generation of the open-state all-points amplitude histograms (bin size 0.2 pA). The resulting peaks on the histogram were fit with Gaussian functions. For kinetic analysis, current records were idealized using a two-point crossing criterion, with the threshold set by eye half-way between blocked and unblocked states. Dwell-time distributions of blocked and unblocked states were generated based on idealized records and fit with a single exponential. The time constants were calculated from the mean dwell time using a method to correct for instrumental dead-time and missed events (Colquhoun and Hawkes, 1995). In the analysis of E*II*Q mutant, the longest transitions to low and high conductance levels observed in several experiments were used to estimate the corresponding current levels. Once determined, these values were used for analysis of all records obtained at the same voltage. The idealized records for the E*II*Q mutant were obtained by a two-point crossing criterion, using two thresholds, one half-way between L and M and another half-way between M and H.

To estimate the frequency of direct H-L transitions in E*II*Q mutant, we performed the following analysis. We reasoned that due to limited frequency resolution in our recording setup (10–90% rise time of 67 μs), direct transitions between H and L levels would appear as H-M-L or L-M-H sequences on idealized records, with just one sampling point (40 ms/point) at the medium level. Quantitative analysis revealed that of all the occurrences of the sequences H-M-L or L-M-H, $\sim$10% contained only one sample point at the medium level. Based on the overall dwell-time distribution of the medium state, at least half of these events could be accounted for by short-lived sojourns in the M state in a sequen-

---

[1]*Abbreviations used in this paper:* CNG, cyclic nucleotide gated; E*I*Q, glutamate to glutamine mutation in the position 383 of rabbit α_{1C}; E*II*Q, glutamate to glutamine mutation in the position 736 of rabbit α_{1C}; E*III*Q, glutamate to glutamine mutation in the position 1145 of rabbit α_{1C}; E*IV*Q, glutamate to glutamine mutation in the position 1446 of rabbit α_{1C}; WT: wild type.

tial H ↔ M ↔ L model. Thus, direct H-L transitions cannot be completely excluded but certainly do not occur frequently.

RESULTS

Clear Resolution of Individual Protonation Events in Expressed L-type Channels

cRNAs encoding L-type Ca^{2+} channels were coinjected into *Xenopus* oocytes as the subunit combination $\alpha_{1C}\beta_{2b}\alpha_2$, and unitary current recordings were obtained using the cell-attached patch configuration 4–7 d after cRNA injection. Fig. 1 shows proton block of the expressed L-type Ca^{2+} channels, recorded with monovalent cations as current carriers. Consistent with published observations with native L-type channels (Prod'hom et al., 1987), the single channel current displayed fast flickery transitions between high conductance and low conductance levels when Na^+ was used as a charge carrier at pH 7.4 (Fig. 1 A, *top*). The previous results indicated that these transitions correspond to binding and unbinding of individual protons to the L-type channel, with the high and low conductance levels corresponding to deprotonated and protonated states of the channel respectively (Prod'hom et al., 1987). Deviations from the predictions of the simple blocking model have been reported (Pietrobon at al., 1989; Prod'hom et al., 1989), but they most likely result from participa-

tion of the buffer in the proton transfer reaction, as was recently shown for proton block of the cyclic nucleotide-gated channels (Root and MacKinnon, 1994). Thus, in the following analysis, pH-dependent transitions between two conductance levels of L-type channel will be interpreted as transitions between protonated and deprotonated states of the channel, in accordance with a simple blocking mechanism.

The resolution of the two conductance states in our experiments was improved when H^+ was replaced by $^2H^+$, a heavier hydrogen ion, due to the isotope effect (Fig. 1 A, *middle*; see Prod'hom et al., 1987). Substitution of K^+ for Na^+·as a charge carrier also slowed down the transitions between these two states (data not shown; Pietrobon et al., 1988). Since we anticipated that some of the L-type channel mutants might produce severe changes in block or unblock rates, we chose to use these effects in combination to optimize the recording conditions for kinetic analysis. Thus, most of our experiments were performed with K^+-^2H_2O (Fig. 1 A, *bottom*). The average time in the protonated state in K^+-^2H_2O was two to threefold longer than that measured in K^+-H_2O, and greater than fivefold longer than that found with Na^+-H_2O. Under these conditions, the individual protonation/deprotonation events were clearly evident as abrupt transitions in the amplitude of the single channel current.
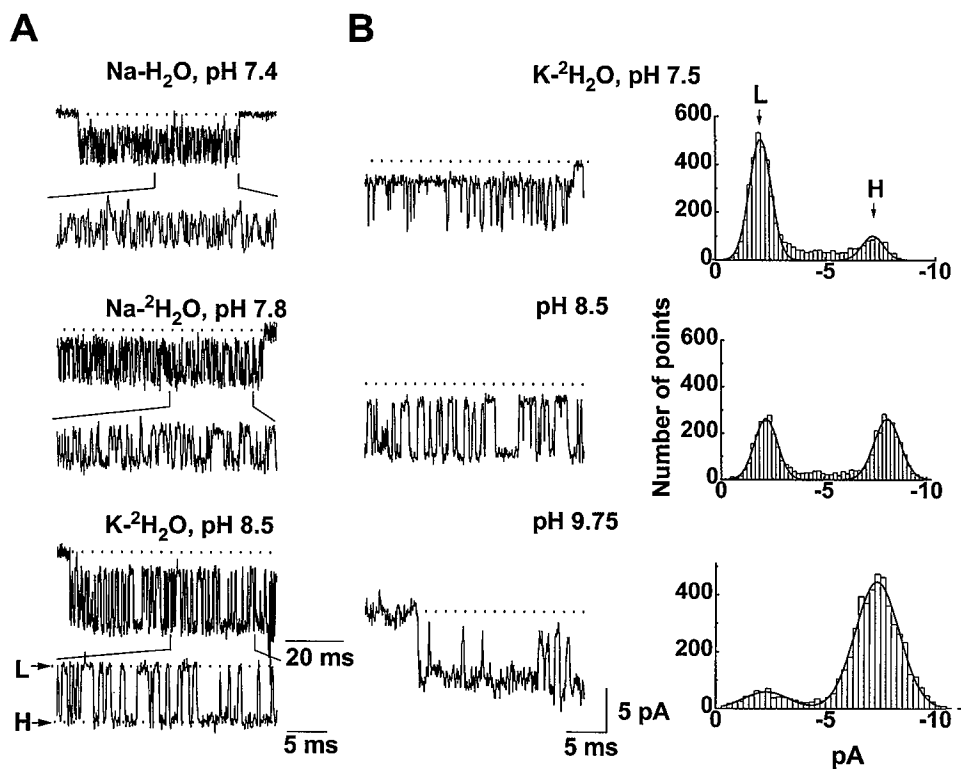
A

Na-H$_2$O, pH 7.4

Na-^{2}H$_2$O, pH 7.8

K-^{2}H$_2$O, pH 8.5

20 ms

L→

H→

5 ms

B

K-^{2}H$_2$O, pH 7.5

pH 8.5

pH 9.75

5 pA

5 ms

FIGURE 1. Proton block of L-type Ca^{2+} channels expressed in *Xenopus* oocytes. (A) The kinetics of proton block were strongly affected by the species of the permeant and blocking ions. Unitary currents recorded in either Na^+-H_2O (−40 mV), Na^+-^2H_2O (−40 mV), or K^+-^2H_2O (−70 mV) are shown on compressed and expanded time scales. Dotted lines mark the closed state or the two conductance levels of the channels. Horizontal arrows indicate the high (*H*) and low (*L*) conductance levels recorded in K^+-^2H_2O (*bottom trace*). (B) The pH dependence of proton block of unitary L-type channel currents. The experiments were performed in K^+-^2H_2O with a −70 mV test potential at indicated external pH values. Representative current traces and open-state all-points amplitude histograms at each pH are shown. The solid curves represent the fitting of the histograms with the sum of two Gaussian functions. Note the shift of the relative areas of the two peaks according to the external pH values.

When the external pH was varied from 7.5 to 9.75, progressive changes were seen in the balance between the high conductance (deprotonated) level and the low conductance (protonated) level (Fig. 1 *B*). Lowering the proton concentration decreased the proportion of time spent in the low conductance state and increased the preponderance of the high conductance state, while not significantly affecting the unitary current amplitude at either level (Fig. 1 *B*, *right*). The slope conductances of the deprotonated and protonated states were 140 ± 23 pS, $n = 4$ and 45 ± 11 pS, $n = 4$ over the range between -120 and -50 mV (Fig. 2 *C*).

To describe the proton block quantitatively, the

open-state all-points amplitude histograms were fitted with the sum of two Gaussian functions (Fig. 1 *B*, *right*, *solid curves*). The unfitted data points between the peaks are due in large part to poorly resolved fast transitions between the blocked and unblocked states. The percentage of block was estimated from the relative areas of the peaks corresponding to protonated (lower conductance) and deprotonated (high conductance) states. The average percentage of time spent in the deprotonated state was $17 \pm 2\%$ ($n = 4$) at pH 7.5; $53 \pm 1.5\%$ ($n = 4$) at pH 8.5; $85 \pm 5\%$ ($n = 2$) at pH 9.75 (Fig. 3 *C*, *WT*). These data are consistent with the presence of a single protonation site with $pK_a \sim 8.5$ under our experimental conditions. Thus, proton block of L-type Ca^{2+} channels expressed in *Xenopus* oocytes (Fig. 1) shares major similarities with that described in guinea pig ventricular myocytes and PC-12 cells (Prod'hom et al., 1987; Pietrobon et al., 1988; Pietrobon et al., 1989; Prod'hom et al., 1989).

Elimination of the High Conductance State in E/Q and E///Q Mutants

To determine whether protonation involves residues within the pore, we analyzed changes in single channel behavior arising from mutations in individual P-region glutamates. We focused on glutamine replacements because they are isosteric and can be regarded as functionally equivalent to permanent protonation. If the protonation site of L-type channels were indeed formed by P-region glutamates, then at least some of the E $\rightarrow$ Q mutations should reduce the single channel current by simulating the protonation of the wild-type channel and alter or occlude the effect of acidic pH by interfering with any additional protonation. These predictions were borne out by the E $\rightarrow$ Q mutation in repeat *I* (E*I*Q), which induced a dramatic change in channel properties (Fig. 2 *A*). Only one current level was apparent in this mutant, the current amplitude histogram conforming to a single Gaussian distribution at either pH 7.5 or 8.5. The corresponding slope conductance was 37 ± 2.5 pS ($n = 4$) over the range between -120 and -50 mV, in good agreement with the slope conductance of the protonated state of the wild-type channel (Fig. 2 C). This result was not restricted to the use of K^+ as a current carrier, as similar observations were made using Na^+ (data not shown). Thus, the E*I*Q mutation not only mimics the effect of protonation on wild-type channel conductance, but also prevents external H^+ from binding to its native site over the pH range tested.

Neutralization of the glutamate in repeat *III* (E*III*Q) also abolished the high conductance level that had been observed in the wild-type channel (Fig. 2 *B*). The major current level for the E*III*Q mutant was characterized by a conductance of 42 ± 3 pS ($n = 3$), similar to the value for E*I*Q and the low conductance level of
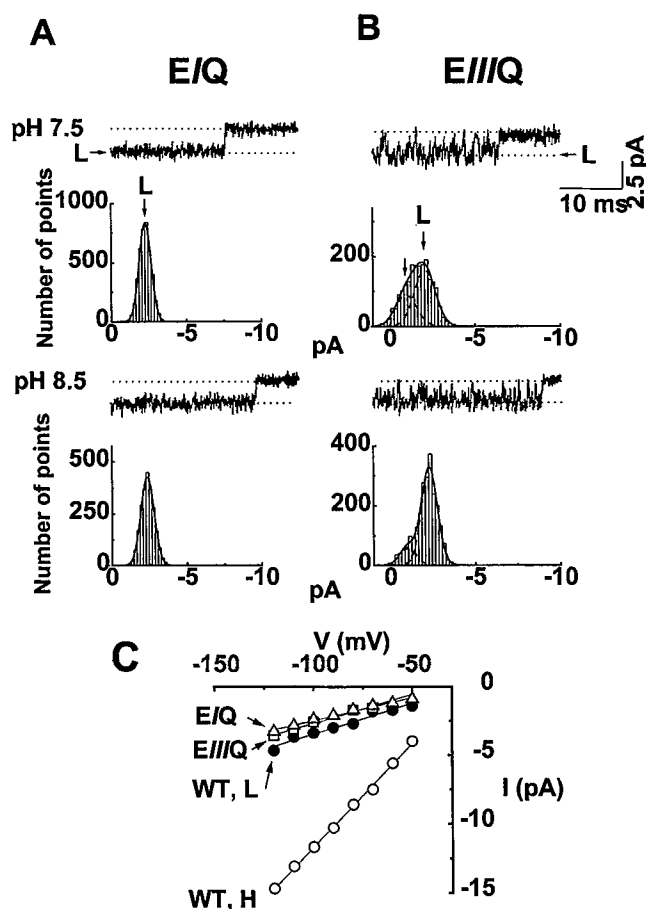

FIGURE 2. E $\rightarrow$ Q mutation in the P-region of repeat *I* and repeat *III* completely abolished the high conductance state. The pH sensitivity of the unitary currents of E*I*Q (*A*) and E*III*Q (*B*) were measured in K^+-^2H_2O at -100 mV. Representative current traces and open-state all points amplitude histograms at indicated pH values. The major conductance level in both mutants is indicated by an arrow. A single Gaussian function was sufficient to fit the open-state amplitude histograms in E*I*Q. In contrast, the sum of two Gaussian functions was required to fit the amplitude histogram of E*III*Q. A combination of reduced current amplitude and increased noise level due to intrinsic patch instability at alkaline pH prevented us from obtaining satisfactory recordings with E*I*Q and E*III*Q mutants at pH 9.75. (*C*) Comparison of the current-voltage relationships for major conductance levels of WT, E*I*Q, and E*III*Q channels.

A pH 8.5

E/VQ

L→
H→

WT

L→
H→

5 pA

10 ms

B E/VQ, pH8.5

Number of points

600
400
200
0

L
H

0   -5   -10
pA

C

% Unblocked

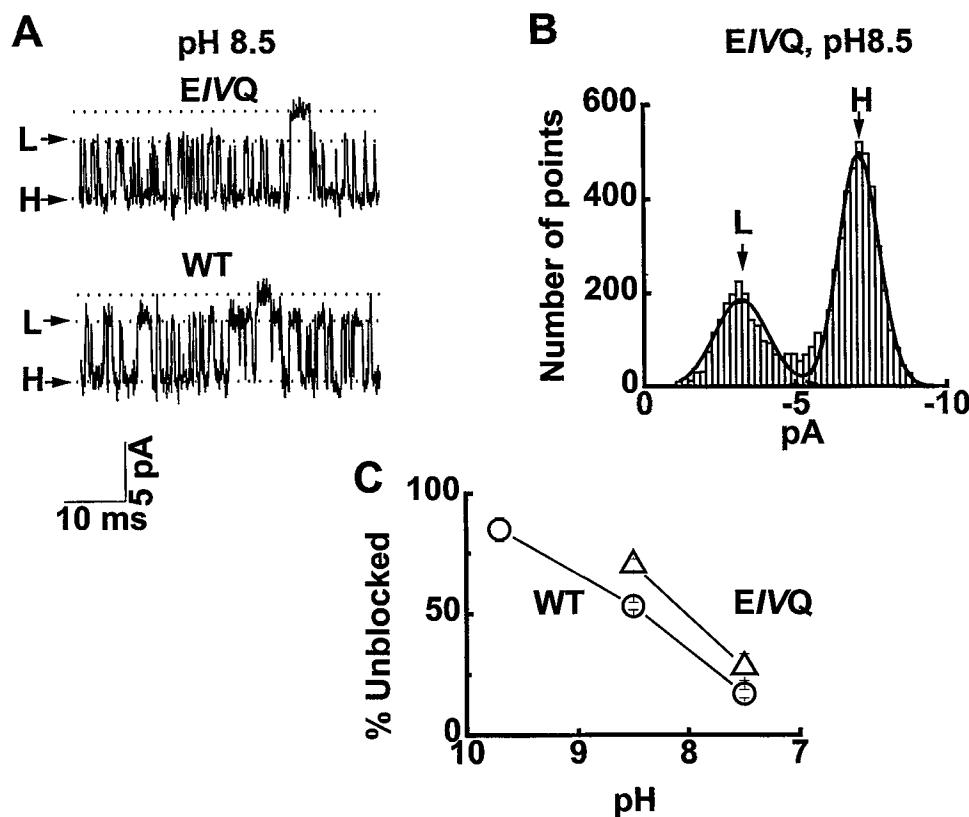100
50
0

WT   E/VQ

10   9   8   7
pH

FIGURE 3. E → Q mutation in the P-region of repeat IV (E/VQ) reduces proton binding affinity without affecting the high (H) and low (L) conductance levels. (A) representative current traces of E/VQ (top) and WT (bottom) recorded at −70 mV at pH 8.5. (B) Open-state all points amplitude histogram of E/VQ. Note difference in relative weights of high (H) and low (L) conductance states relative to WT at the same pH (Fig. 1 B, right). (C) pH dependence of blockade by external H^+ of WT (open circles) and E/VQ (open triangles). The relative occupancy of the unblocked state (% unblocked, ordinate) was estimated from the fractional area under the corresponding Gaussian fit.

wild-type channels (Fig. 2 C). However, unlike E/Q, E/IIQ also displayed fast flickery transitions toward an even lower but apparently non-zero current level that was very small (<1 pA at −100 mV) and readily confused with channel closures due to gating. Examination of current records obtained at −120 and −140 mV confirmed the existence of a lower conductance state (data not shown). Because of this additional level, two Gaussian functions were required to fit the open channel, all-points amplitude histogram of E/IIQ mutant (Fig. 1 B). Since the relative areas of the corresponding peaks were affected by variation of external pH (Fig. 2 B), we concluded that transitions to the lower conductance level in E/IIQ mutant correspond to protonation events. The pK_a appeared to be <7.5 because even at this pH, channels spend <50% of the time in the protonated state. Evidently, the E/IIQ mutation mimics the effect of normal protonation on the single channel conductance for monovalent cations, without eliminating the possibility of additional protonation by external H^+ ions.

Destabilization of the Protonated State in the E/VQ Mutant

The E → Q mutation in repeat IV (E/VQ) resulted in a much milder alteration in channel behavior (Fig. 3). This mutation did not prevent blockade by external protons or alter significantly the conductances of either deprotonated and protonated states relative to wild-

type channels (Fig. 3 A, and see Fig. 7 B). However, the degree of blockade at pH 8.5 was only 30 ± 2.4% (n = 4) in the E/VQ mutant (Fig. 3 B), compared to 47 ± 1.5% (n = 4) in WT (Fig. 1 B). Compared to the WT channel, the pH$_o$-dependence of the fraction of time spent in the unblocked state was shifted in the acidic direction in the E/VQ mutant (Fig. 3 C), corresponding to a change in pK_a from 8.5 (WT) to 8.2 (E/VQ).

Kinetic analysis illuminated the mechanism of pK_a changes in the E/VQ mutant (Fig. 4). Dwell-time distributions of the unblocked and blocked states of WT channels and the E/VQ mutant were generated from idealized records and fitted with single exponentials. Fig. 4 B shows a comparison of dwell time distributions and the corresponding exponential fits obtained for E/VQ (solid lines) and WT channels (dashed lines) at pH 8.5. It is evident that the mean blocked time was significantly reduced in the E/VQ mutant compared to WT, without a significant change in the mean unblocked time.

Using a conventional procedure to correct for instrumental dead-time and missed events (Colquhoun and Hawkes, 1995), we estimated the dwell time constants for the WT channel and the E/VQ mutant at two different external proton concentrations (Fig. 4 C). At pH 8.5, the corrected dwell time in the deprotonated (unblocked) state was 0.48 ± 0.03 ms (n = 4) for the WT channel and 0.40 ± 0.08 ms (n = 4) for E/VQ, not significantly different (P > 0.05). In contrast, comparison

A

Blocked time

Unblocked time

5 pA

2.5 ms

B

Number of events

Unblocked

WT - -
E/VQ—

Blocked

Duration (ms)

Duration (ms)

C

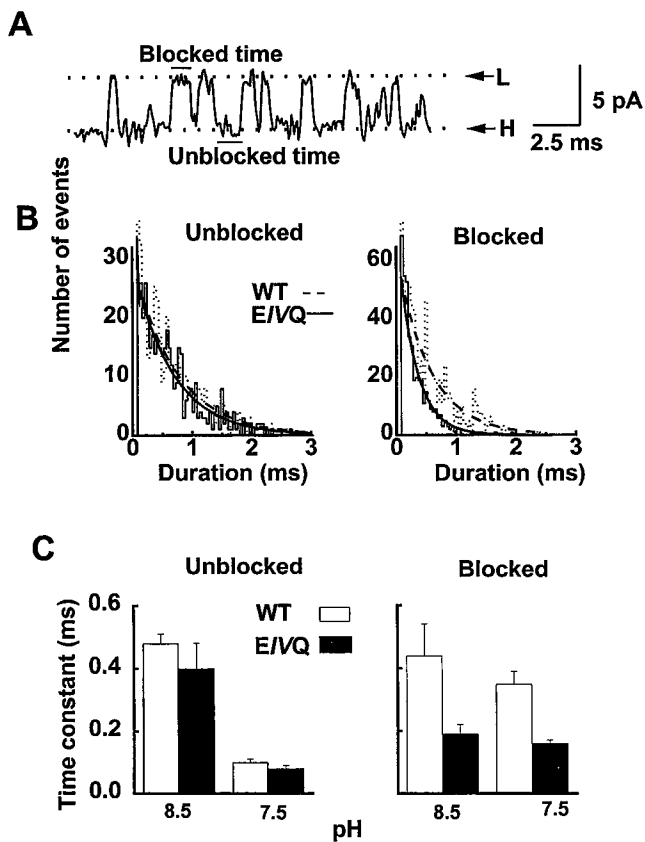Time constant (ms)

Unblocked

WT ☐
E/VQ ■

Blocked

pH

FIGURE 4. Reduction of proton binding affinity in E/VQ mutant was due to acceleration of the proton off-rate. (A) An example of blocked time and unblocked time measurements used to generate dwell time distributions. (B) Comparison of block-unblock kinetics of E/VQ (*solid lines*) and WT channels (*dashed lines*) at pH 8.5. The dwell-time distributions were generated from idealized current traces and fitted with single exponentials. (C) The pH dependence of dwell time constants, $\tau_{unblocked}$ (*left*) and $\tau_{blocked}$ (*right*). Data are given for WT channels (*open bars*) and the E/VQ mutant (*solid bars*). The time constants were calculated from the mean dwell times using a method to correct for instrumental dead-time and missed events (Colquhoun and Hawkes, 1995).

of the corrected dwell time of the protonated (blocked) state gave values of 0.44 ± 0.1 ms (*n* = 4) for WT and 0.19 ± 0.03 ms (*n* = 4) in the E/VQ mutant, a significant reduction (*P* < 0.001, unpaired *t* test). Similar results were obtained at pH 7.5 (Fig. 4 C). Thus, the reduction in pK_a in the E/VQ mutant was due to an approximately twofold increase in the rate of deprotonation ($\tau_{blocked}^{-1}$), with no significant change in the protonation rate ($\tau_{unblocked}^{-1}$). According to analysis of dwell-time distributions in the unblocked state (Fig. 4 C), a 10-fold increase in proton concentration yields a five-fold change in the rates of protonation for both WT channel and E/VQ mutant. Possible explanations of the <10-fold increase in rate include the participation of pH buffer in the proton transfer reaction (see Root and MacKinnon, 1994) or pH-dependent changes in the local surface potential near the mouth of the channel.

We concluded from these results that the protonation site is essentially intact in the E/VQ mutant. While the side-chain carboxylate of the glutamate in repeat *IV* has no detectable influence on access of protons to the site (lack of effect on blocking rate), it helps to stabilize the bound proton, most likely via through-space electrostatic interaction. The stabilizing influence of E/V, revealed by an increase in proton off rate in the E/VQ mutant, can be interpreted in terms of an electrostatic interaction that deepens the energy well for the bound proton in WT channel compared with E/VQ. The energy of this interaction (ΔE) may be simply estimated as $\Delta E = kT\ln(K_{off}^{E/VQ}/K_{off}^{WT})$, or 0.61 kT based on our data. This translates into a change of 16 mV in the local electrical potential experienced by the bound proton due to the E/VQ mutation. For a Coulombic interaction, the 16 mV change would correspond to a distance between the proton and the E/V carboxylate of at least 11 Å, since the effective dielectric constant in the channel pore (ε) must be <80 (Dudley et al., 1996).

The Appearance of Three Conductance Levels in the E//Q Mutant

The effect of the E → Q mutation in repeat *II* was the most surprising. Unlike the wild-type channel and the other point mutants, the E//Q mutant displayed three distinct current levels, high (H), medium (M), and low (L). These are readily apparent in the voltage range between −70 and −120 mV (Fig. 5 A), and correspond to three distinct slope conductances in plots of the voltage-dependence of unitary current amplitude (Fig. 5 B). The medium conductance level (102 ± 2 pS, *n* = 3) was not found with any of the other mutant channels or WT, but appeared to be predominant in the E//Q mutant at pH 8.5 (Fig. 5 A). The low conductance level in this mutant (53 ± 1 pS, *n* = 3) was close to the protonated state of the WT channel. Most of the transitions to the high conductance level were too brief to allow a precise measurement of the current amplitude (Fig. 5 A). However, a rough estimate of the conductance for this state based on current amplitudes of relatively long-lived events was ~145 pS, close to the value for the deprotonated state of the wild-type channel.

Detailed analysis of the kinetic relationships between three conductance states in E//Q mutant was begun by idealization of unitary current recordings (Fig. 5 A, bottom trace; see METHODS for details). Examination of such records suggested that direct transitions between high and low conductance states occurred rarely compared to those in the sequence H ↔ M ↔ L (see METHODS for details).

To determine whether any of the transitions involved protonation/deprotonation steps, we examined the pH-dependence of the relative occupancy of the three conductance states (Fig. 6). Open channel all-points
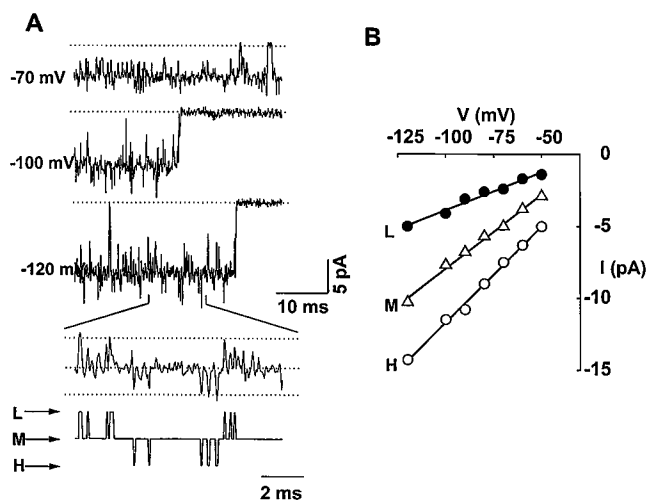
A

B

V (mV)
-125 -100 -75 -50

L

M

H

I (pA)

10 ms

5 pA

2 ms

L→
M→
H→

FIGURE 5. Appearance of three conductance states in an E → Q mutation in the P-region of repeat II (E//Q). (A) Examples of current traces of the E//Q mutant obtained at indicated voltages from a representative experiment (pH 8.5). A portion of the record at −120 mV and its corresponding idealized trace are shown on an expanded time scale. The three open conductance levels (high, H; medium, M; low, L) are indicated by arrows. (B) Current-voltage relationships of the three conductance states.

to the H state were too brief and infrequent to justify fitting the corresponding bins on the amplitude histogram with a third Gaussian function. To compare relative occupancies of all three conductance states at different pH values, current records were idealized as previously described (Fig. 5 A), and the proportion of channel open time spent at various conductance levels was determined from individual idealized sweeps, then averaged across multiple sweeps and experiments. At pH 8.5, the E//Q mutant channel spends 5.5 ± 0.6% of its open time at the high conductance level, 83.1 ± 0.5% at the medium level, and 11.4 ± 0.1% at the lowest level ($n = 3$, Fig. 6 B). The probability of the low conductance state was elevated to 34% at pH 7.5, and reduced to 3.3% at pH 9.75 (Fig. 6 B), whereas occupancy of the medium conductance state showed opposite effects. Thus, the low conductance is likely to correspond to a protonated state, and the medium conductance to a deprotonated state.

In contrast to the M ↔ L equilibrium, the ratio of H and M occupancies remained at ∼0.06 over the pH range from 9.75 to 7.5. This indicates that transitions between high and medium states do not involve protonation/deprotonation steps. As an additional test, we compared the behavior of the E//Q mutant in ^2H_2O and H_2O solutions, but found no significant difference in kinetics of transitions between high and medium conductances (data not shown). This runs contrary to the isotope effect that would be expected if this transition corresponded to a protonation event. The lack of
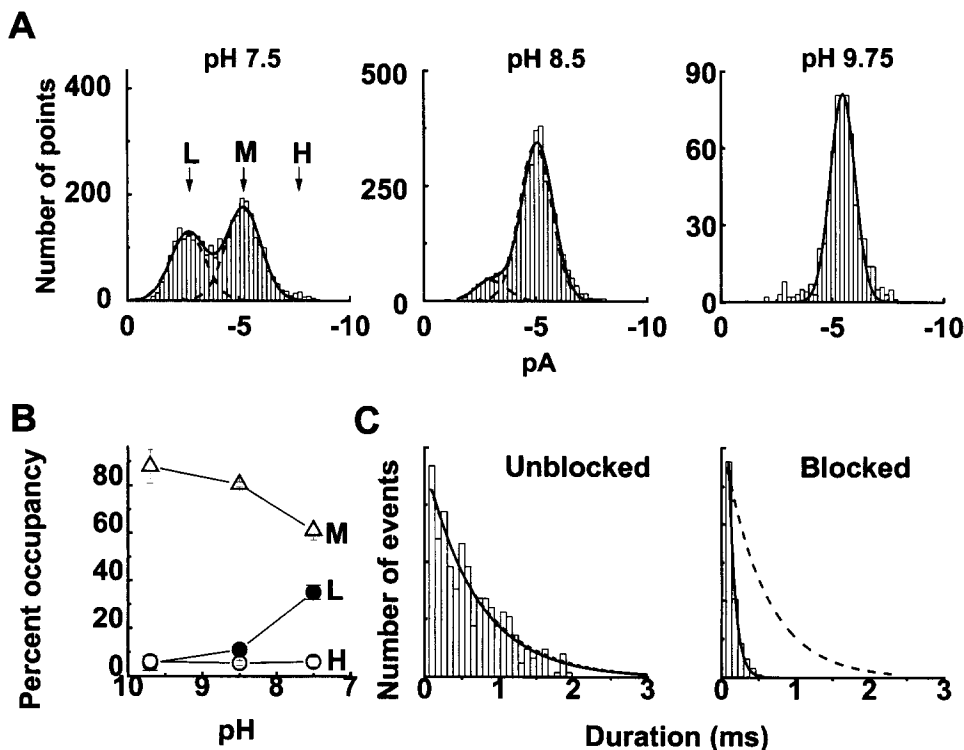
amplitude histograms of the E//Q mutant at −70 mV were generated at the pH values as indicated. The data were fitted with a sum of two Gaussian functions, corresponding to medium and low levels. The balance between M and L conductance states was clearly affected by variation of extracellular pH (Fig. 6 A). Transitions

A

pH 7.5

Number of points

400

200

0

L   M   H

0   -5   -10

pH 8.5

500

250

0

0   -5   -10

pA

pH 9.75

90

60

30

0

0   -5   -10

B

Percent occupancy

80

60

40

20

0

M

L

H

10   9   8   7

pH

C

Number of events

Unblocked

0   1   2   3

Blocked

0   1   2   3

Duration (ms)

FIGURE 6. The pH sensitivity of the three-conductance states in the E//Q mutant. (A) Open-state all-points amplitude histograms at indicated values of pH. The amplitude histograms were fitted with a sum of two Gaussian functions (solid curves), corresponding to M and L conductance states. (B) The pH dependence of the percent occupancy of the three conductances. (C) The dwell time distribution of the low conductance state, pH 8.5. The dashed line shows an exponential fit to WT data at the same pH.

pH-dependence of the H ↔ M transition implies that the E*II*Q mutant channel can undergo changes between these two conductance levels without net entry or exit of protons.

The affinity of the protonated (low conductance) state in the E*II*Q mutant was substantially reduced (pK_a < 7.5) as compared to wild-type channel (pK_a ~ 8.5) under the same ionic conditions (Fig. 6, *A* and *B*). A kinetic analysis of the dwell-time distribution of the low conductance state revealed that the weaker proton affinity of the E*II*Q mutant was associated with a greater than fivefold faster off-rate of bound H^+ as compared to WT (Fig. 6 *C*), based on values of the uncorrected mean blocked time. Correction for missed events was not possible because the observed mean blocked time was very close to instrumental dead time (80 μs). It is clear, nonetheless, that bound protons were destabilized much more severely in the E*II*Q mutant than in E*IV*Q. If the influence of E*II* on the bound proton were to be assumed purely electrostatic, a distance of >4.4 Å between the bound proton and a fully ionized E*II* may be estimated according to the simple electrostatic considerations described above.

DISCUSSION

By combining the approaches of site-directed mutagenesis and single channel recording, we have demonstrated that proton block of Ca^{2+} channels involves a subset of the same conserved P-region glutamates which govern Ca^{2+} selectivity. Because these amino acids have been conclusively localized to the permeation pathway (Kim et al., 1993; Tang et al., 1993; Yang et al., 1993; Ellinor et al., 1995), these experiments strongly support a direct interaction between protons and a site within the Ca^{2+} channel pore, not outside as it has been previously proposed (Pietrobon et al., 1989). Our results highlight notable differences between proton block of Ca^{2+} channels and other types of cation channels, as discussed below. The observed interactions between H^+ ions and pore mutants provide a novel perspective on the disposition of the P-region glutamates and their specific roles in supporting ion selectivity and permeation.

Each E → Q Mutation Produces a Unique Effect on Proton Block

Each of the P-region glutamates appears to play a distinct role in promoting the intrapore protonation, in line with its asymmetrical contribution to selective interactions with Ca^{2+} and other divalent cations (Kim et al., 1993; Tang et al., 1993; Yang et al., 1993; Ellinor et al., 1995). The E*I*Q construct showed the sharpest difference in behavior in comparison to native channels. Two findings are particularly interesting: first, E*I*Q dis-

played only one current level, whose conductance was in close agreement with that of the protonated state of WT channels (Figs. 2 *C* and 7), and second, this mutant was completely unresponsive to changes in pH over a range that strongly affected WT channels (Fig. 2 *A*). These conclusions can be stated quite strongly because the single channel recordings would be capable of resolving even brief and infrequent sojourns at the high conductance level. The combination of results would be difficult to explain if the protonation were to take place at a site separate from E*I*, which the glutamine substitution had left intact. In such a scenario, mutations might be expected to shift the pH-dependence but not to abolish the deprotonated conductance level in entirety. On the other hand, the ability of the E*I*Q mutant to mimic and occlude H^+-dependent block is exactly the result expected if E*I* were directly involved in forming the protonation site: the glutamine substitution for glutamate can be regarded as equivalent to permanently affixing a proton to the carboxylate side chain. This represents compelling evidence that E*I* is titrated during the protonation event, and therefore, that the H^+ binding site lies within the pore. Accordingly, the well-described dependence of proton block on the permeant ion species (Pietrobon et al., 1989; Prod'hom et al., 1989; Kuo and Hess, 1993; Klockner and Isenberg, 1994) is readily explained without invoking an allosteric mechanism (Pietrobon et al., 1989).

Like E*I*Q, E*III*Q completely lacked the high conductance level corresponding to the deprotonated state in WT channels. Evidently, glutamine substitutions in motif III and motif I can exert a similar effect on monovalent cation permeation. However, one notable difference is that further protonation is possible for E*III*Q, as indicated by flickery reductions in current to an even lower level (Fig. 2 *B*). We were unable to study these events in full detail, but it was clear that the reductions in conductance were pH-dependent, albeit over a more acidic range of pH than WT channels. One interpretation that we have considered is that the E*III*Q replacement spares some possibility of protonation of E*I*, while markedly shifting the pK_a in the acidic direction.

In contrast to E*I*Q and E*III*Q, the glutamine replacement mutants in motifs II and IV both retained high and low conductance states, although the H^+ affinity of E*II*Q and E*IV*Q was reduced relative to WT. The difference between E*IV*Q and WT was relatively mild, an approximately twofold decrease in proton affinity (Fig. 3 *C*), suggesting that E*IV* played only a limited role in stabilizing the bound H^+. The change in affinity was accounted for by an increased off-rate of the titratable proton, while the on-rate was hardly affected (Fig. 4). A change in the on-rate would have been expected on the basis of changes in local $[H^+]$ if E*IV* were in ionized form and located on the extracellular side of the pro-
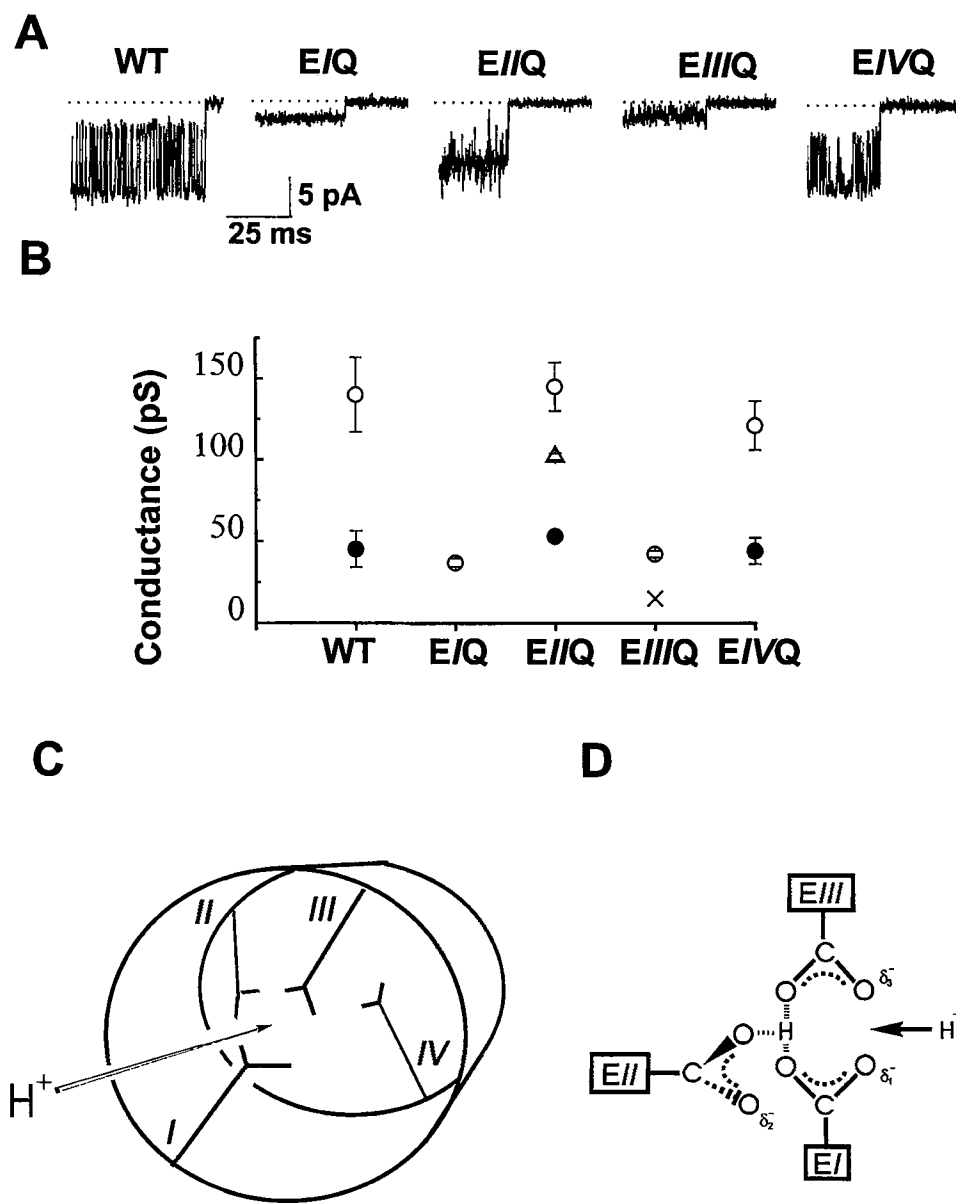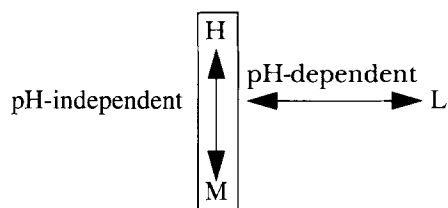
A WT   E/Q   E//Q   E///Q   E/VQ

5 pA

25 ms

B

Conductance (pS)

C   **D**

FIGURE 7. Comparison of behavior of individual E → Q mutants and a proposed structural model of how P-region glutamates form the proton-binding site of L-type Ca^{2+} channels. (A) Representative single channel recordings of WT and E → Q mutants at −100 mV and pH 8.5. (B) Summary of slope conductances of WT and the four E → Q mutants. The slope conductances of each mutant were obtained from I-V curves over the range between −50 and −120 mV at pH 8.5 and 7.5. Points are plotted as mean ± SD ($n \geq 3$). Open symbols, deprotonated states; filled symbols, protonated states. The existence of a protonated state with reduced conductance in the E///Q mutant is indicated by ×. (C) A schematic drawing of a proposed arrangement of the four P-region glutamates and the structure of the protonation site in the L-type channel. (D) A three-centered H-bond arrangement as one possible configuration of the complex of E/, E//, and E/// in its deprotonated state.

ton binding site. The simplest explanation of our data is that E/V is positioned on the cytoplasmic side of the site. Other lines of evidence provide independent support for this interpretation. Parent and Gopalakrishnan (1995) replaced E/V with less bulky amino acids and found systematic increases in monovalent conductance, as if this residue acted as a final bottleneck for ion permeation. Furthermore, Sather et al. (1994) showed that alanine substitution for E/V has no detectable effect on the on-rate for block by external Cd^{2+}. Thus, E/V appears to be less externally accessible than other P-region glutamates, being located further downstream along the permeation pathway (cf., Tang et al., 1993; Yang et al., 1993). If one presumes that E/V stabilizes protonation by a through-space electrostatic interaction, we calculate that its negative charge must

be >10 Å from the titration site (see RESULTS). Notably, the alanine residue at the homologous position of repeat IV of Na^+ channels has also been suggested to lie further along the permeation path than homologous P-region residues in other repeats (Chiamvimonvat et al., 1996), consistent with the overall structural similarity between voltage-gated Ca^{2+} and Na^+ channels.

The E//Q mutation displayed a third conductance level, between the H and L levels, the dominant conducting state of this construct over a wide range of pH. The emergence of this intermediate conductance was quite striking since it was not found in WT or any of the other glutamine substitution mutants. In interpreting the M conductance, a key finding was that while its prevalence relative to the low conductance was pH dependent, its prevalence relative to the high conductance was

not (Fig. 6 B). Thus, the relationship between the conductance states can be diagrammed as follows:

$$\text{pH-independent} \quad \boxed{\begin{array}{c} \text{H} \\ \uparrow \\ \downarrow \\ \text{M} \end{array}} \quad \xrightarrow[\text{pH-dependent}]{\longleftrightarrow} \text{L}$$

We speculate that the H and M states correspond to two distinct configurations of the P-region glutamate side chains, rendered distinguishable by the E*II*Q mutation. Since the proton affinity of E*II*Q was >10-fold lower than WT, the E*II* side chain is also likely to be closely associated with the proton binding site, much more so than E*IV*.

A Model to Explain Distinctive Features of the Ca²⁺ Channel Protonation Site

Our experiments highlight notable distinctions between H⁺ block of Ca²⁺ channels, Na⁺ channels, and cyclic nucleotide-gated (CNG) channels. We found that H⁺ block of mutant or wild-type Ca²⁺ channels involved one protonation reaction at most (see also Prod'hom et al., 1987). In contrast, CNG channels display two independent and identical intrapore titration sites for protons (Root and MacKinnon, 1994). The difference in behavior is particularly intriguing because the CNG channel pore is thought to contain four glutamate residues in equivalent positions that form a high-affinity Ca²⁺ binding site (Root and MacKinnon, 1993), very much like the Ca²⁺ channel. The most striking difference between Ca²⁺ channels and Na⁺ channels lies in their apparent H⁺ affinity. The pK$_a$ of the protonation site at the extracellular mouth of Na⁺ channels is 4.6–4.9 (Woodhull, 1973; Mozhayeva et al., 1981; Zhang and Siegelbaum, 1991; Daumas and Andersen, 1993), close to the pK$_a$ expected for a single glutamate carboxylate (~4.4). In contrast, the pK$_a$ of the protonation site within Ca²⁺ channels (and both of the sites in CNG channels) is more than three log units higher.

Here we propose a model to explain how the four glutamic acid side chains in Ca²⁺ channels give rise to single protonation site rather than two or more, with a H⁺ affinity >10³-fold greater than a typical carboxylate. Our results lead us to hypothesize that the protonation site is formed by E*I*, acting in conjunction with E*III* and to a lesser extent, E*II*, while E*IV* influences protonation much less directly from a vantage point further along the permeation pathway (Fig. 7 C). In this model, the critical carboxylates take on H⁺ ions and are linked together by hydrogen bonds, which minimizes the energetic cost of positioning several negatively charged oxygen groups in close proximity in the absence of diva-

lent cations. Hydrogen bonding networks among multiple carboxylates are quite common in proteins, often exerting a stabilizing force between adjacent subunits; multiple hydrogen-bonded carboxylates can exhibit a much higher pK$_a$ than unpaired carboxylates (Sawyer and James, 1982). Hydrogen-bonding between neighboring oxygen groups has been proposed previously for CNG channels, albeit in the form of carboxylic acid-carboxylate pairs (Root and MacKinnon, 1994). In contrast, concerted action of multiple carboxylate side chains is unlikely to occur in Na⁺ channels, in which the P-region positions corresponding to residues E*I*-E*IV* are occupied by Asp, Glu, Lys, and Ala (Heinemann et al., 1992). Pairing of the positively charged lysine with one of the acid residues would leave only one carboxylate free as a titratable group, thus accounting for the much lower H⁺ affinity of Na⁺ channels relative to Ca²⁺ channels.

We believe that the distinctive characteristics of Ca²⁺ channel protonation arise from the concerted action of the trio of E*I*, E*II*, and E*III* and that this configuration provides a much more satisfactory account of our observations than arrangements in which E*I* and other glutamates act alone or pairwise. For illustrative purposes, we put forward a speculative scenario in Fig. 7 D. In the deprotonated state of the complex, the three carboxylate side chains are held together by a permanently shared H⁺ in a three-centered H-bond configuration (Jeffrey and Saenger, 1991). The complex bears a net charge of −2 and thus offers great attraction for entry of an external proton (indicated by *arrow*). This electrostatic interaction helps explain the unusually high pK$_a$ of the Ca²⁺ channel site. In the deprotonated state, E*I* and E*III* are likely to be transiently complexed to a monovalent cation or to be tilted out of plane due to electrostatic repulsion between the oxygens, which bear partial negative charge. Once H⁺ enters the site, it is shared between E*I* and E*III*, allowing these side chains to become coplanar; the symmetry of the resulting carboxyl–carboxyl complex contributes further to the high pK$_a$. The reduction in negative charge due to protonation would be expected to decrease the rate of monovalent cation flux, thus producing a subconductance state.

How might this model account for the E*I*Q and E*III*Q phenotypes? Substitution of an -NH₂ for an -O on either E*I* and E*III* would neutralize the side chain, acting in lieu of a titratable H⁺, resulting in formation of an N-H··O hydrogen bond or formation of alternative carboxyl–carboxylate pairs that were not present in the WT. We suggest that, for either E*I* or E*III*, charge neutralization would mimic the effect of protonation in driving the channel out of the high conductance state. On the other hand, we speculate that E*I* and E*III* might be expected to differ in whether the glutamine replace-

ment abolished all possibility of protonation, depending on geometrical position of these side chains in the channel pore or their chemical interaction with EII side chain or other neighboring residues. It is likely that EI is involved in additional protonation in EIIIQ mutant, leading to the expectation that simultaneous glutamine substitution for both EI and EIII would produce extremely small unitary currents, like those seen with the protonated state of EIIIQ. Indeed, oocytes expressing the EIQ-EIIIQ double mutant have shown small Ba^{2+} currents in whole-cell recordings and no clear unitary K^{+} currents in preliminary cell-attached recordings. This seems consistent with the hypothesis, but we cannot yet exclude the possibility that expression of the EIQ-EIIIQ construct is simply inefficient.

Possible Insights into the Mechanism of Ca^{2+} Permeation

H^{+} interactions provided a novel perspective on the behavior of the pore glutamates, useful in understanding their participation in Ca^{2+} selectivity and permeation. The proposed apposition of P-region glutamates *I*, *II*, and *III* is of great interest, not only as a possible high-affinity protonation site, but also because it represents an array of oxygen groups not unlike those found in high-affinity Ca^{2+} binding sites of known three-dimensional structure (Falke et al., 1994). There are clues that arrival of a divalent cation at the glutamate locus might cause some rearrangement in its configuration. For example, while EIV has only mild influence on H^{+} block in the absence of Ca^{2+}, mutations at this position affect Ca^{2+} and Cd^{2+} block to a far greater extent than could be explained by a through-space electrostatic interaction (Kim et al., 1993; Tang et al., 1993; Yang et al., 1993; Ellinor et al., 1995). This disparity would make sense if Ca^{2+} interaction with the EI-EII-EIII complex allowed the EIV carboxylate to swing into position to provide additional coordination for the divalent cation. As discussed above, an additional hint of conformational freedom in the P-region glutamates was provided by the behavior of the EIIQ mutant, which displayed pH-independent transitions between high and medium conductances. The proposed rearrangements provide examples of what might be possible when the pore accommodates multiple Ca^{2+} ions. Conformational flexibility in the glutamate locus may be particu-

larly important as a mechanism for mediating ion–ion interactions, thereby allowing the pore to support high rates of divalent cation transfer (Tsien et al., 1987; Armstrong and Neyton, 1992; Kuo and Hess, 1993; Yang et al., 1993).

Physiological Implications of Proton Regulation of Ca^{2+} Influx

These results provide a molecular basis for an important regulatory function of extracellular pH: the control of ion flux through open Ca^{2+} channels. The steeply pH$_o$-dependent reduction of unitary current will help decrease the overall Ca^{2+} influx, together with reduced channel open probability (Prod'hom et al., 1987; Krafte and Kass, 1988; Klöckner and Isenberg, 1994). Our experiments provide a simple and satisfying explanation for the antagonism between H^{+} and Ca^{2+}. At physiological [Ca^{2+}]$_o$, competition for pore glutamates will strongly influence the pK$_a$ for protons, thus explaining why changes in external pH in the vicinity of pH 7 produce such marked effects on voltage-gated Ca^{2+} current (Krafte and Kass, 1988; Pietrobon et al., 1989; Klockner and Isenberg, 1994) and K^{+}-induced Ca^{2+} entry (Ou-Yang et al., 1994). The inhibition of Ca^{2+} entry by H^{+} will exert a substantial effect in the modulation of cell excitability during vigorous neuronal activity (Chesler and Kaila, 1992) and the promotion of cell survival during epileptic seizures and short-term cerebral or cardiac ischemia (Katz, 1992; Siesjo et al., 1993).

Because the P-region glutamates are perfectly conserved in all known α$_1$ subunits of voltage-gated Ca^{2+} channels, pronounced pH-sensitivity is likely to be a universal characteristic of this family of membrane proteins. This is in contrast to NMDA receptor channels, whose regulation by pH$_o$ (Traynelis and Cull-Candy, 1991) is markedly dependent on a specific RNA splice variation, in exon 5 (Traynelis et al., 1995). Unlike voltage-gated Ca^{2+} channels, NMDA receptors respond to external acidification not by a reduction in open channel current but strictly by decreased likelihood of channel opening (Traynelis and Cull-Candy, 1991). Thus, the two major pathways for synaptically driven Ca^{2+} entry show similar overall responsiveness to pH$_o$ but by fundamentally different molecular mechanisms.

REFERENCES

Armstrong, C.M., and J. Neyton. 1992. Ion permeation through calcium channels: a one-site model. *Ann. NY Acad. Sci.* 635:18–25.

Chesler, M., and K. Kaila. 1992. Modulation of pH by neuronal activity. *TINS (Trends Neurosci.).* 15:396–402.

Chaimvimonvat, N., M.T. Pérez-Garcia, R. Ranjan, E. Marban, and G.F. Tomaselli. 1996. Depth Asymmetries of the pore-lining segments of Na⁺ channel revealed by cysteine mutagenesis. *Neuron.* 16:1037–1047.

Colquhoun, D., and A.G. Hawkes. 1995. The principle of the stochastic interpretation of ion-channel mechanisms. *In* Single Channel Recording, 2nd Ed., B. Sakmann and E. Neher, editors, Plenum, New York, 397–482.

Coulter, K.L., F. Perier, C.M. Radeke, and C.A. Vandenberg. 1995. Identification and molecular localization of a pH-sensing domain for the inward rectifier potassium channel HIR. *Neuron.* 15:1157–1168.

Daumas, P., and O.S. Andersen. 1993. Proton block of rat brain sodium channels. *J. Gen. Physiol.* 101:27–43.

Dudley, S.C., J.L. Penzotti, G. Lipkind, R.J. French, and H.A. Fozzard. 1996. A specific energetic coupling suggests the orientation of μ-conotoxin GIIIA with respect to the Na⁺ channel outer vestibule. *Biophys. J.* 70:A23.

Ellinor, P.T., J. Yang, W.A. Sather, J.-F. Zhang, and R.W. Tsien. 1995. Ca²⁺ channel selectivity at a single locus for high-affinity Ca²⁺ interactions. *Neuron.* 15:1121–1132.

Falke, J.J., S.K. Drake, A.L. Hazard, and O.B. Peersen. 1994. Molecular tuning of ion binding to calcium signaling proteins. *Q. Rev. Biophys.* 27:219–290.

Heinemann, S.H., H. Teriau, W. Stuhmer, K. Imoto, and S. Numa. 1992. Calcium channel characteristics conferred on the sodium channel by single mutations. *Nature (Lond.).* 356:441–443.

Hille, B. 1992. Ionic Channels of Excitable Membranes, 2nd Ed., Sinauer Associates, Sunderland, MA.

Hullin, R., D. Singer-Lahat, M. Freichel, M. Biel, N. Dascal, F. Hofmann, and V. Flockerzi. 1992. Calcium channel beta subunit heterogeneity: functional expression of cloned cDNA from heart, aorta and brain. *EMBO (Eur. Mol. Biol. Organ.) J.* 11:885–890.

Jeffrey, G.A., and W. Saenger. 1991. Hydrogen Bonding in Biological Structures. Springer-Verlag, Berlin.

Katz, A.M. 1992. Physiology of the Heart. 2nd Ed., Raven Press, New York.

Kim, M.S., T. Morii, L.X. Sun, K. Imoto, and Y. Mori. 1993. Structural determinants of ion selectivity in brain calcium channel. *FEBS Lett.* 318:145–148.

Klöckner, U., and G. Isenberg. 1994. Calcium channel current of vascular smooth muscle cells: extracellular protons modulate gating and single channel conductance. *J. Gen. Physiol.* 103:665–678.

Krafte, D.S., and R.S. Kass. 1988. Hydrogen ion modulation of Ca channel current in cardiac ventricular cells. Evidence of multiple mechanisms. *J. Gen. Physiol.* 91:641–657.

Kuo, C.C., and P. Hess. 1993. Characterization of the high-affinity Ca²⁺ binding sites in the L-type Ca²⁺ channel pore in rat phaeochromocytoma cells. *J. Physiol. (Lond.).* 466:657–682.

Methfessel, C., V. Witzemann, T. Takahashi, M. Mishina, S. Numa, and B. Sakmann. 1986. Patch clamp measurements on *Xenopus laevis* oocytes: currents through endogenous channels. *Pflugers Arch.* 407:577–588.

Mikami, A., K. Imoto, T. Tanabe, T. Niidome, Y. Mori, H. Takeshima, S. Narumiya, and S. Numa. 1989. Primary structure and functional expression of the cardiac dihydropyridine-sensitive calcium channel. *Nature (Lond.).* 340:230–233.

Mozhayeva, G.N., A.P. Naumov, and Y.A. Negulyaev. 1981. Evidence for existence of two acid groups controlling the conductance of sodium channel. *Biochim. Biophys. Acta.* 643:251–255.

Ou-Yang, Y., T. Kristian, P. Mellergard, and B.K. Siesjo. 1994. The influence of pH on glutamate- and depolarization-induced increases of intracellular calcium concentration in cortical neurons in primary culture. *Brain Res.* 646:65–72.

Parent, L., and M. Gopalakrishnan. 1995. Glutamate substitution in repeat *IV* alters divalent and monovalent cation permeation in the heart Ca²⁺ channel. *Biophys. J.* 69:1801–1813.

Perrin, D.D., and B. Dempsey. 1974. Buffers for pH and Metal Ion Control. Chapman and Hall, London.

Pietrobon, D., B. Prod'hom, and P. Hess. 1988. Conformational changes associated with ion permeation in L-type calcium channels. 333:373–376.

Pietrobon, D., B. Prod'hom, and P. Hess. 1989. Interactions of protons with single open L-type calcium channels. *J. Gen. Physiol.* 94:1–21.

Prod'hom, B., D. Pietrobon, and P. Hess. 1987. Direct measurement of proton transfer rates to a group controlling the dihydropyridine-sensitive Ca²⁺ channel. *Nature (Lond.).* 329:243–246.

Prod'hom, B., D. Pietrobon, and P. Hess. 1989. Interactions of protons with single open L-type calcium channels. *J. Gen. Physiol.* 94:23–42.

Root, M.J., and R. MacKinnon. 1993. Identification of an external divalent cation-binding site in the pore of a cGMP-activated channel. *Neuron.* 11:459–466.

Root, M.J., and R. MacKinnon. 1994. Two identical noninteracting sites in an ion channel revealed by proton transfer. *Science (Wash. DC).* 265:1852–1856.

Sather, W.A., I. Nussinovich, D.J. Gross, J. Yang, and R.W. Tsien. 1994. Changes in single Ca²⁺ channel properties produced by mutations in the L-type channel pore. *Biophys. J.* 66:A128.

Sather, W.A., T. Tanabe, J.-F. Zhang, Y. Mori, M.E. Adams, and R.W. Tsien. 1993. Distinctive biophysical and pharmacological properties of class A (BI) calcium channel α₁ subunits. *Neuron.* 11:291–303.

Sawyer, L., and M.N.G. James. 1982. Carboxyl-carboxylate interaction in proteins. *Nature (Lond.).* 295:79–81.

Siesjo, B.K., K. Katsura, P. Mellergard, A. Ekholm, J. Lundgren, and M.L. Smith. 1993. Acidosis-related brain damage. *Prog. Brain Res.* 96:23–48.

Tang, S., G. Mikala, A. Bahinski, A. Yatani, G. Varadi, and A. Schwartz. 1993. Molecular localization of ion selectivity sites within the pore of a human L-type cardiac calcium channel. *J. Biol. Chem.* 268:13026–13029.

Traynelis, S.F. 1996. pH modulation of ligand-gated ion channels. *In* pH and Brain Function. K. Kaila and B.R. Ransom, editors. John Wiley and Sons, New York. In press.

Traynelis, S.F., and S.G. Cull-Candy. 1991. Pharmacological properties and H⁺ sensitivity of excitatory amino acid receptor channels in rat cerebellar granule neurones. *J. Physiol. (Lond.).* 433:727–763.

Traynelis, S.F., M. Hartley, and S.F. Heinemann. 1995. Control of proton sensitivity of the NMDA receptor by RNA splicing and polyamines. *Science (Wash. DC).* 268:873–876.

Tsien, R.W., P. Hess, E.W. McCleskey, and R.L. Rosenberg. 1987. Calcium channels: mechanisms of selectivity, permeation, and block. *Annu. Rev. Biophys. Biophys. Chem.* 16:265–290.

Woodhull, A.M. 1973. Ionic blockage of sodium channels in nerve. *J. Gen. Physiol.* 61:687–708.

Yang, J., P.T. Ellinor, W.A. Sather, J.-F. Zhang, and R.W. Tsien. 1993. Molecular determinants of Ca selectivity and ion permeation in L-type Ca channels. *Nature (Lond.).* 366:158–161.

Zhang, J.-F., and S.A. Siegelbaum. 1991. Effects of external protons on single cardiac sodium channels from guinea pig ventricular myocytes. *J. Gen. Physiol.* 98:1065–1083.